JOURNAL OF QUATERNARY SCIENCE (2020) 1–10 ISSN 0267-8179. DOI: 10.1002/jqs.3250

JQS Journal of Quaternary Science QRA Quaternary Research Association

Holocene records of eolian dust deposition from high-elevation lakes in the Uinta Mountains, Utah, USA

JEFFREY S. MUNROE,* RYAN McELROY, SAM O'KEEFE, ANDREW PETERS and LUNA WASSON
Geology Department, Middlebury College, Middlebury, VT, USA

Received 13 July 2020; Revised 28 August 2020; Accepted 6 September 2020

ABSTRACT: Radiocarbon-dated sediment cores from subalpine lakes were used to investigate post-glacial dust deposition in the Uinta Mountains (Utah, USA). Lake sediments were geochemically characterized with ICP-OES, ICP-MS and XRF core scanning. Collections from passive samplers constrain the properties of modern dust, and samples of regolith constrain properties of the local material within the watershed. Ca and Eu are more abundant in dust, whereas Ti and Zr are more abundant in local regolith. As a result, the Ca/Ti and Eu/Zr ratios are indices for the dust content of lake sediment. In all records, the dust index rises in the early Holocene as watersheds became stabilized with vegetation, reducing the influx of local material. After this point, values remained above average through the middle Holocene, consistent with an increased dust content in the sediment. Dust index values drop in the late Holocene in most lakes, suggesting a decrease in dust abundance. Generally synchronous shifts in dust index values in cores from lakes in different parts of this mountain range are evidence of enhanced dust deposition in this region during the middle Holocene, and are consistent with a variety of records for increased aridity in the south-western USA at this time. Copyright © 2020 John Wiley & Sons, Ltd.

KEYWORDS: dust; geochemistry; Holocene; limnology; Uinta Mountains

Introduction

The deposition of eolian dust is increasingly recognized as a significant factor in the functioning of mountain ecosystems. Fine-grained sediment eroded by wind, transported through the atmosphere, and deposited through both wet and dry mechanisms represents an important delivery of exotic material to the mountain critical zone (Lawrence *et al.*, 2013; Aciego *et al.*, 2017; Arvin *et al.*, 2017). Accumulation of dust over geologic time exerts a strong control on pedogenic pathways of mountain soils (Litaor, 1987; Dahms, 1993; Muhs and Benedict, 2006; Lawrence *et al.*, 2011; Munroe *et al.*, 2015). In the shorter term, nutrients provided by dust influence the productivity of mountain lakes and streams (Ballantyne *et al.*, 2011; Brahney *et al.*, 2014, 2013). Most immediately, the deposition of dust lowers the albedo of mountain snowpack (Skiles *et al.*, 2015; Skiles and Painter, 2017). This darkened snow melts more rapidly, with impact on both the timing and the magnitude of the nival flood downstream (Painter *et al.*, 2007, 2010; Skiles *et al.*, 2012).

At the same time, dust deposition is the downwind expression of processes operating in dust source areas. These processes include climatic change, development of mineral crusts on playas and other sparsely vegetated landscapes, and both natural and anthropogenic surface disturbances, all of which can alter the amount of fine-grained material available for wind entrainment (Urban *et al.*, 2009; Flagg *et al.*, 2014; Duniway *et al.*, 2019). Therefore, dust deposition is both an important component of mountain geoecology, as well as a long-distance signal of conditions in dust source regions.

Considerable research has focused on characterizing the properties of modern dust in mountain environments (Goodman *et al.*, 2019; Heindel *et al.*, 2020), measuring dust fluxes (Lawrence and Neff, 2009; Munroe, 2014), evaluating the effects of dust deposition (Aciego *et al.*, 2017; Skiles *et al.*, 2018; Rea *et al.*, 2020) and ascertaining the sources of this dust (Munroe *et al.*, 2019; Kandakji *et al.*, 2020; Nicoll *et al.*, 2020). A smaller number of studies have considered changes in dust deposition over time, in part because continuous archives of dust deposition in mountain environments are rare. Although many alpine soils are capped by layers of loess (Litaor, 1987), bio- and cryoturbation effectively incorporate this material into the solum (Muhs and Benedict, 2006; Munroe, 2007). As a result, thick deposits of loess, which are significant archives of Quaternary climate change elsewhere in the world (Roe, 2009), are unusual in high-elevation settings. The few studies that have attempted to reconstruct dust fluxes over time have generally relied on lake sediments. A seminal paper utilizing this approach identified a major anthropogenic component to latest Holocene dust deposition in Colorado (Neff *et al.*, 2008). More recently, studies have presented dust flux reconstructions farther back into the Holocene (Routson *et al.*, 2016, 2019; Arcusa *et al.*, 2020). All of these efforts are significant for the way in which they synthesize observations of modern dust with paleorecords. However, given the scarcity of Holocene-length records, the importance of dust deposition in mountain environments, and how dust deposition connects the mountains to upwind source areas in which effective moisture has varied during the postglacial period, more records are needed to understand how dust deposition has changed over longer stretches of time.

The present study generated Holocene-length records of dust deposition from lake sediment cores collected in the Uinta Mountains of Utah, USA. These mountains are located downwind of extensive arid landscapes in south-western North America that serve as regional dust sources (Reynolds *et al.*, 2016; Nicoll *et al.*, 2020), and specific areas in Utah, Nevada and Arizona have been identified as likely sources for much of the modern dust arriving in the Uintas (Munroe *et al.*, 2019). Previous work has also demonstrated the

*Correspondence: Jeffrey S. Munroe, as above.
E-mail: jmunroe@middlebury.edu

significant geoecological role played by long-term dust deposition in these mountains (Bockheim *et al.*, 2000; Munroe, 2007). Here, cores collected as part of a larger study (Munroe and Laabs, 2020) were analyzed geochemically with a variety of methods. Collections were also made of modern dust and regolith, and a geochemical fingerprint was identified to distinguish between dust and local material. This fingerprint was then applied to the lake sediment cores to determine how the abundance of dust in lake sediment changed over time.

Methods

Setting

This research was conducted in the Uinta Mountains, part of the Rocky Mountain system in north-eastern Utah, USA (Fig. 1). Bedrock of the Uinta Mountains (hereafter, the 'Uintas') is a sequence of Precambrian quartzite, sandstone and argillite that was uplifted during the Laramide Orogeny (Bradley, 1936; Sears *et al.*, 1982; Dehler *et al.*, 2007). Summit elevations reach >4 km above sea level, and the range exhibits classic alpine glacial geomorphology indicating the presence of more than 2000 km^2 of glacial ice during the Last Glacial Maximum (Munroe and Laabs, 2009). Cosmogenic ^{10}Be surface-exposure dating indicates that glaciers began to retreat around 18 000 years ago (Munroe *et al.*, 2006; Laabs *et al.*, 2009), and although small glaciers may have occupied sheltered cirques during the Younger Dryas stade in the latest Pleistocene (Munroe and Laabs, 2017), no glaciers are present in these mountains today. Lakes, ranging in area from <1 to >70 ha, are abundant within the area covered by active ice during the last glaciation (Atwood, 1908, 1909). These lakes are surrounded by a variety of vegetation communities including *Pinus contorta* (lodgepole pine) forest at intermediate elevations, *Picea engelmannii* (Engelmann spruce) and *Abies lasiocarpa* (subalpine fir) in the upper-subalpine forest, and alpine tundra featuring *Acomastylis rossii* (alpine avens) and *Polygonum bistortoides* (alpine bistort) above ~3300 m (Shaw and Long, 2007; Munroe, 2012). The Uinta climate is characterized by long, snowy winters and cool summers. Mean annual precipitation ranges from 500 to 925 mm, with more than 60% falling as snow at elevations >3300 m asl (Munroe and Mickelson, 2002; Munroe, 2003). Mean annual air temperature above ~3100 m asl is <0 °C (Munroe, 2006, 2007; Bockheim and Munroe, 2014).

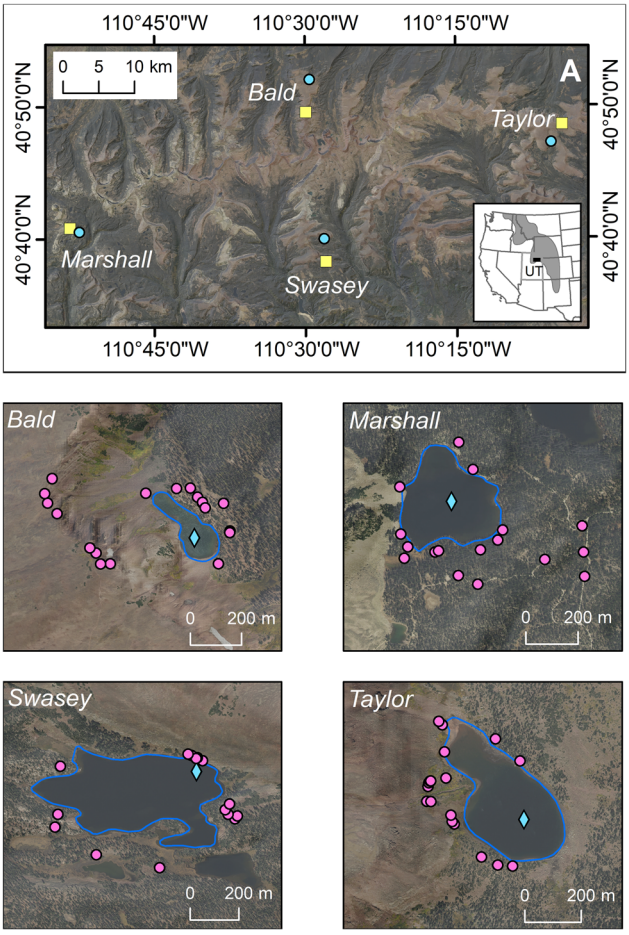

Figure 1. Location map of the study area in the Uinta Mountains. Inset shows the location of the Uinta Mountains (black box) in north-eastern Utah (UT). The gray polygon delineates the Rocky Mountain province in the western USA. Larger figure shows a true color image of the Uinta Mountains with the four study areas identified. Yellow boxes identify the dust collectors, and blue circles represent the lakes. Lower figures present enlargements of the area around each lake. The pink circles mark local regolith samples, and the blue diamond represents the coring location. [Color figure can be viewed at wileyonlinelibrary.com]

Fieldwork

The sediment cores in this study were collected in 2004 and 2005 as detailed by Munroe and Laabs (2020). Briefly, coring sites were selected with a bathymetric survey to identify a location in deep water, away from inlets or steep slopes (terrestrial and subaqueous) that could deliver sediment through mass wasting. A percussion corer (Reasoner, 1993) was used with a 6-m-long barrel of 7.5-cm-diameter PVC pipe. It is not possible to collect unconsolidated near-surface sediment with this technique, and therefore all records are artificially truncated at a depth of ~50 cm.

Cores from four lakes were studied: Bald, Marshall, Swasey and Taylor (Figs 1 and 2). These lakes are located from 3043 to 3421 m asl, have an average depth of ~10 m, and range from 2.2 ha (Bald) to 21.7 ha (Swasey) in area (Table 1). These particular lakes were selected because they represent different sectors of the Uinta Mountains, and because each is located near a passive sampler constraining properties of modern dust (Fig. 1). Details of these samplers have been presented (Munroe, 2014; Munroe *et al.*, 2015), but each is a ~50 × 50-cm tray of glass beads that collects dust through wet and dry deposition. The samplers, which have been in continuous operation since 2011, are emptied by washing the dust from the beads with distilled water.

Finally, to characterize the regolith in the watersheds surrounding the cored lakes, samples of relatively unweathered deep (BC or C horizon) material were collected from hand excavations and tree-tip mounds in 2015 and 2016 (Fig. 1). Deep material was prioritized to avoid the dust-derived silt cap present at the top of most Uinta soil profiles (Bockheim and Koerner, 1997; Bockheim *et al.*, 2000; Munroe, 2007).

Laboratory analyses

All sediment cores were analyzed for standard physical and chemical properties at 1-cm resolution, including grain size distribution, water content, loss on ignition (LOI) and C:N ratio, as detailed in Munroe and Laabs (2020). Age control was provided by radiocarbon dating of terrestrial macrofossils (Munroe and Laabs, 2020), and depth–age models were developed using CLAM (Blaauw, 2010). For Swasey and Taylor lakes, initial analyses, including radiocarbon dating, were conducted on one core, and geochemical analyses were conducted on a parallel core collected at the same time from the same point in the lake. LOI analysis was conducted on

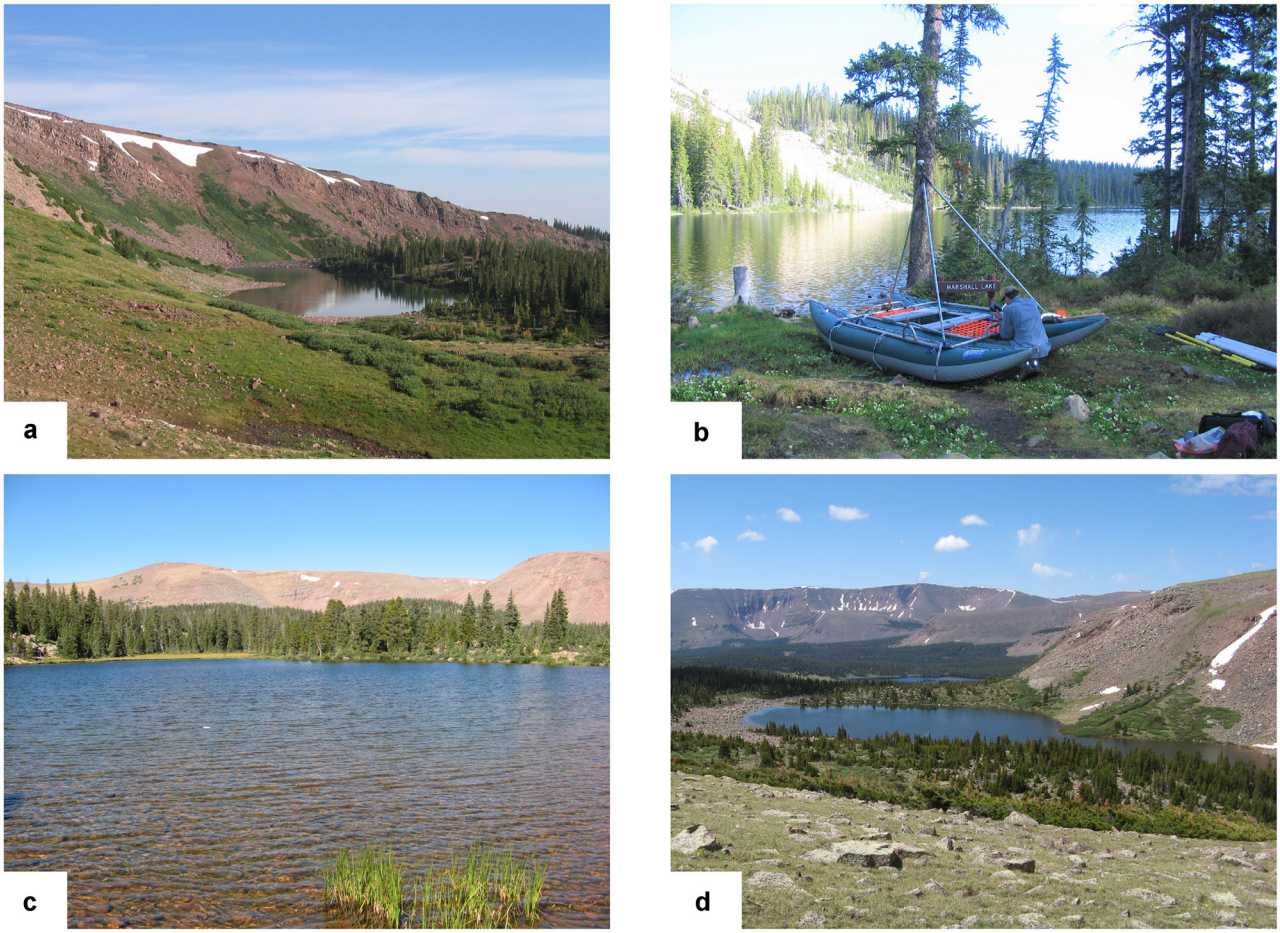

Figure 2. Pictures of the lakes cored in this study. (a) Bald Lake; (b) Marshall Lake, showing the coring platform; (c) Swasey Lake; (d) Taylor Lake, showing the debris fan mentioned in the text (right). [Color figure can be viewed at wileyonlinelibrary.com]

both cores, and the resulting LOI time series were matched to transpose the depth–age model from the first core to the second.

Geochemical analysis of the cores was conducted using several methods. Discrete subsamples of the core from Marshall Lake (2-cm spacing) were analyzed for major and some trace elements using inductively coupled plasma optical emission spectrometry (ICP–OES). The core from Bald Lake was analyzed for trace elements using a Thermo iCAP Q inductively coupled mass emission spectrometry (ICP-MS) device on 3-cm-thick contiguous samples. In both cases, samples were ignited and fluxed with lithium metaborate before dissolution in HNO_3. Calibration curves were generated with in-house standard solutions, and internal standards were analyzed after every five samples for drift correction. USGS rock standard RGM-1 was measured at the beginning and end of every set of samples as an overall check on results. The cores from Swasey and Taylor Lakes were analyzed for major and trace elements using an ITRAX X-ray fluorescence (XRF) core scanner at the University of Massachusetts – Amherst. Scans were made using an Mo tube at a resolution of 2 mm and a count time of 10 s. System voltage was set to 60 kV, and current was set to 50 mA during the analyses. As a check for consistency, the core from Swasey Lake was reanalyzed on the same instrument 2 years later, using a voltage of 40 kV and a current of 10 mA, again with 2-mm spacing.

Dust samples were processed following established procedures including centrifuging, and treatment with H_2O_2 to remove organic matter (Munroe, 2014; Munroe *et al.*, 2015, 2019). Samples of local regolith were prepared by slaking ~100 cm^3 of the <2-mm fraction in Nanopure water. Following disaggregation (3–7 days), samples were dispersed and settled in accordance with Stoke's law to yield a grain size distribution matching the sediments in the corresponding lake core. Samples of dust and the settled fraction of the local regolith were ignited and ground to a powder before submission for ICP-MS analysis at SGS Minerals following according to protocol GE-ICM-90A.

Table 1. Locations and dimensions of the cored lakes.

Lake ID*	Lake name	Latitude N	Longitude W	Elevation (m)	Water depth (m)	Lake area (ha)	A_W/A_L†	Core length (cm)
04-01	Marshall	40°40.538	110°52.452	3043	10.7	8.0	7.5	190
04-06	Swasey	40°40.048	110°28.000	3267	9.5	14.6	21.7	198
05-06	Bald	40°52.030	110°29.540	3367	7.0	2.2	14.5	355
05-10	Taylor	40°47.193	110°05.478	3421	11.0	9.0	35.4	270

*Lake ID given by Munroe and Laabs (2020).
†Ratio of watershed area to lake area.

f-

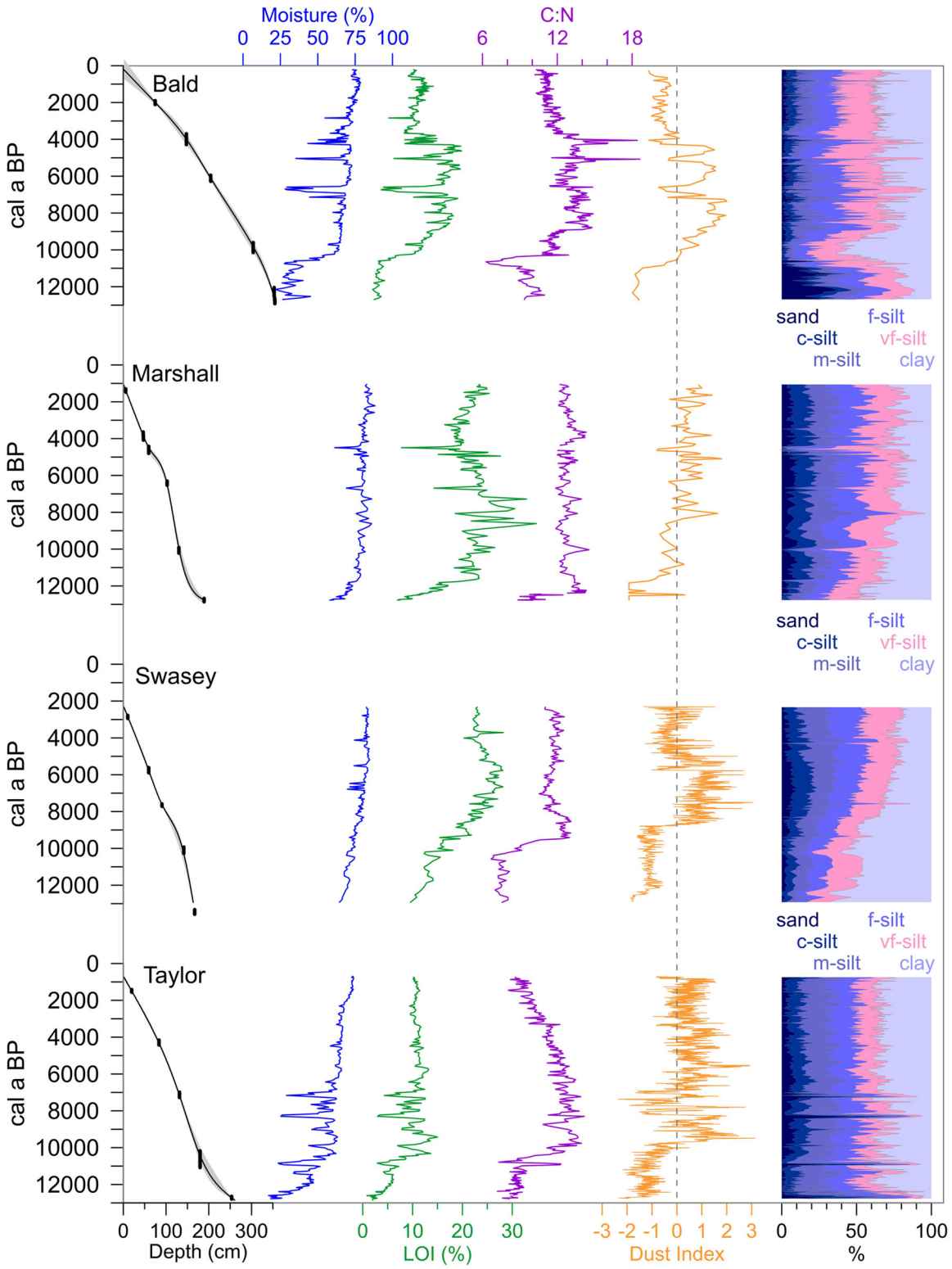

Figure 3. Composite plot of properties measured in the sediment cores from Bald, Marshall, Swasey and Taylor Lakes. Depth–age models (with narrow uncertainty envelopes in gray) were developed in CLAM (Blaauw, 2010). Solid black lines denote the calibration ranges for the ^{14}C ages supporting the age models. Moisture content and loss-on-ignition (LOI) were determined with a thermogravimetric analyzer (Dean, 1974). C:N was measured with an elemental analyzer. Grain size distribution with silt fractions was determined with laser scattering. Details of these methods are presented in Munroe and Laabs (2020). The dust index values are normalized elemental ratios sensitive to the dust content of the lake sediment, as discussed in the text. The dashed vertical line denotes 0 on the normalized scale. [Color figure can be viewed at wileyonlinelibrary.com]

Nature of the sedimentary records

The cores analyzed in this study consist of two broadly contrasting types of sediment. Upper sections are massive gyttja ranging from black where organic content is high, to pinkish or gray in low-organic sections depending on the color of the surrounding bedrock. In contrast, basal sediments eature alternating millimetre- to centimetre-scale layers of relatively coarse sand and dense clay that are devoid of visible organic material. Details of the sedimentology of these cores are presented in Munroe and Laabs (2020).

On the basis of the radiocarbon-based age models (Munroe and Laabs, 2020), the sediment cores extend back to ~12.8k cal a BP (Fig. 3). Because unconsolidated sediment was lost

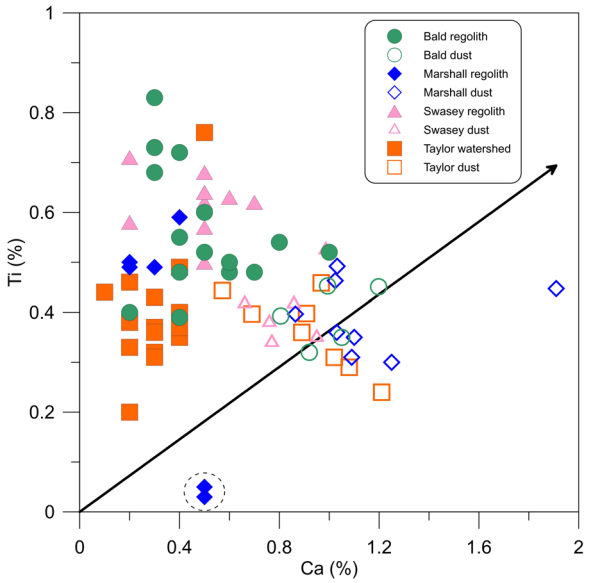

Figure 4. Scatterplot of Ca and Ti abundance in samples of dust and regolith grouped by watershed. The black arrow delineates a linear regression through the origin and the regolith samples. The two samples circled at the bottom were quartz arenites collected from talus near Marshall Lake. [Color figure can be viewed at wileyonlinelibrary.com]

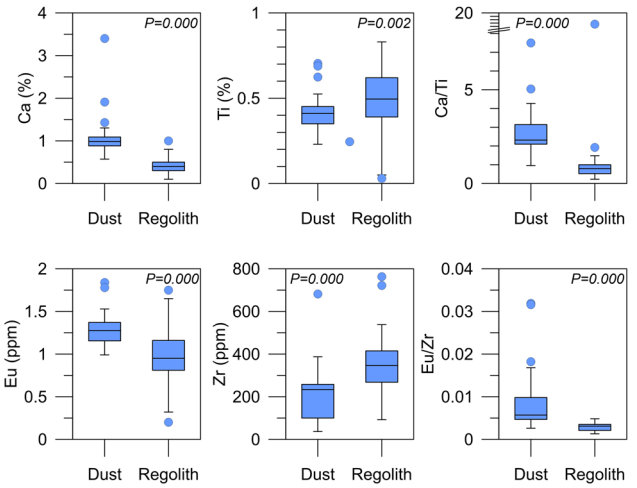

Figure 5. Boxplots of Ca, Ti, Eu and Zr abundances in modern dust and regolith used in calculating the dust indices Ca/Ti and Eu/Zr. The *p*-values for the difference between dust and regolith were determined with a Mann–Whitney test. [Color figure can be viewed at wileyonlinelibrary.com]

from the top of the cores during retrieval, none of the records reach the present, even though sedimentation is clearly an ongoing process in each lake. Collectively, the four records overlap across most of the Holocene (Fig. 3).

Measurements of water content, LOI, C:N and grain size distribution exhibit similarities and differences between the records (Fig. 3). Water content is greatest in the cores from Swasey and Marshall Lakes, corresponding to higher LOI. Time series of LOI feature a long-duration rising and falling pattern in the cores from Bald, Marshall and Swasey Lakes, whereas values of LOI generally fluctuate around a constant mean in the core from Taylor Lake. The cores from Bald and Taylor Lakes feature numerous thin (1–5 cm) layers of mineral-rich sediment, which are characterized by low water content and LOI. Values of C:N reach an early high (ca. 10k cal a BP) in Taylor Lake before steadily falling. C:N in Swasey Lake also reaches a high ca. 10k cal a BP, but after falling slightly remains stable from 8 to 2k cal a BP. C:N is stable throughout the record from Marshall Lake, whereas values of C:N are more variable in the core from Bald Lake. Grain size distributions in all four cores are dominated by silt and clay, with only minor amounts of sand except in the basal section from Bald Lake. Clay is significant in the early part of the records from Marshall and Swasey Lakes, but decreases in abundance over time.

Development of a dust index

Given their small size, simple geometries and undeveloped watersheds, the fine fraction of the clastic sediment accumulating in the studied lakes is a mixture of exotic dust and local regolith. Accordingly, a dimensionless geochemical dust index was developed to characterize the abundance of dust in the lake sediments. Although a large number of elements were detected in the cores, the dust and local regolith, because different methodologies were used in analyzing these samples, the suite of elements assayed was not consistent. Therefore, in developing a dust index, emphasis was placed upon elements which were analyzed in as many types of samples as possible. The abundances of these elements were investigated to identify those that are significantly more abundant in dust relative to local regolith, or more abundant in regolith relative to dust. The significance of differences was evaluated using a Mann–Whitney test. A ratio between such elements would be proportional to the abundance of dust in the lake sediment. Working with ratios also avoided closed-sum effects, and permitted consideration of the results from the XRF core scanner, which are reported in X-ray intensity, rather than direct elemental concentration. Additionally, previous work has revealed that some elements are unusually abundant in modern lake sediments and dust because of anthropogenic activity (Reynolds *et al.*, 2010; Munroe, 2014). These elements were excluded in developing the dust index.

After applying these criteria, the most widely applicable formulation of a dust index is the ratio between Ca and Ti. Ca is significantly more abundant in modern dust samples (Figs 4 and 5; Table 2), yet the abundance of Ca did not increase as a result of anthropogenic activity over the past two centuries (Reynolds *et al.*, 2010). Although the common Ca-bearing mineral calcite has not been detected in Uinta dust, the dust does contain substantial plagioclase (Munroe, 2014; Munroe *et al.*, 2015), a mineral which is not present at detectable levels in Uinta bedrock and regolith. Conversely, Ti is significantly more abundant in samples of regolith (Figs 4 and 5; Table 2). Ti occurs in rutile, sphene and other oxides with high specific gravity, and is chemically immobile in surface environments. As a result, Ti tends to accumulate in weathering sediments over time (Nesbitt and Markovics, 1997), and is not typically transported long distances by eolian processes. The Ca/Ti ratio in Uinta lake sediment should therefore be proportional to the amount of dust in the lake sediment relative to material derived from local regolith.

A different approach was required for Bald Lake because although trace elements were measured throughout this core, major elements were only quantified for a subset (~20%) of samples with ICP-MS. Instead, the Eu/Zr ratio is used as a dust index. Similar to Ca, the trace element Eu is significantly more abundant in dust relative to local regolith (Fig. 5; Table 2), and Eu often substitutes for Ca in plagioclase (McLennan, 1989). At the same time, Zr is significantly more abundant in regolith (Fig. 5; Table 2), and is also immobile under surface weathering conditions. In the subset of samples for which both major and trace elements were analyzed, Ca and Eu are strongly correlated, as are Ti and Zr ($p = 0.000$). As a result, the Eu/Zr ratio can be interpreted in the same way as Ca/Ti (Fig. 5).

Table 2. Geochemical measurements for dust and regolith samples used in the development of a dust index.

	Ca (%)		Ti (%)		Ca/Ti		Eu (p.p.m.)		Zr (p.p.m.)		Eu/Zr	
	Dust	Regolith	Dust	Regolith	Dust	Regolith	Dust	Regolith	Dust	Regolith	Dust	Regolith
Mean	1.05	0.39	0.41	0.50	2.72	1.28	1.28	0.98	208.57	359.31	0.0084	0.0029
Median	0.99	0.40	0.41	0.50	2.32	0.79	1.28	0.95	233.51	346.00	0.0057	0.0031
SD	0.45	0.18	0.10	0.16	1.16	2.60	0.19	0.33	117.28	125.63	0.0068	0.0009
Variance	0.20	0.03	0.01	0.03	1.34	6.74	0.04	0.11	13 753.62	15 781.68	0.0000	0.0000
Range	2.83	0.90	0.47	0.80	6.55	16.44	0.85	1.55	644.88	670.40	0.0293	0.0035
Minimum	0.57	0.10	0.23	0.03	0.95	0.23	0.99	0.20	37.00	92.60	0.0026	0.0013
Maximum	3.40	1.00	0.70	0.83	7.50	16.67	1.84	1.75	681.88	763.00	0.0319	0.0048
Count	40	50	42	50	40	50	39	50	42	50	39	50

However, because Eu was not measured with the XRF scanner for the cores from Swasey and Taylor Lakes, or for Marshall Lake with ICP-OES, the Eu/Zr ratio cannot be applied to all four lacustrine records.

As a final step, to standardize the dust indices for the separate lake sediment records, values of Ca/Ti (Marshall, Swasey and Taylor Lakes) and Eu/Zr (Bald Lake) were converted to a *z*-score based on the mean and standard deviation for the individual cores.

Dust index variations over time

As displayed in Fig. 3, the dust index in each core varies over time. In general, values are below average in the early part of each record, are higher in the middle Holocene and decrease again towards the top. Often, increases in dust index are not synchronous with other major changes in measured sedimentary properties. For instance, in the cores from Swasey and Taylor Lakes the prominent rise in dust index in the early Holocene occurs ~1000 years after the onset of increasing LOI and C:N values. By contrast, the increase in dust index occurs at essentially the same time as the rise in LOI in the core from Bald Lake. Overall, there is no consistent relationship between dust index values and sediment grain size distribution, and there is no correspondence between changes in dust index and sedimentation rates, revealed as the slope of the depth–age model (Fig. 3).

Closer comparison of the dust index time series is possible in Fig. 6, where the records are presented on the same timescale. In all cores the dust index rises above average between 10 and 9k cal a BP. The onset of this increase occurs ca. 11k cal a BP in Bald, Marshall and Taylor Lakes, and later in Swasey Lake (ca. 9k cal a BP). This offset is puzzling, because if the dust index is tracking dust deposition, then shifts in dust index should be synchronous in all the lakes. By contrast, regolith in watersheds that became vegetated earlier would have stabilized earlier, reducing the amount of local material available for transport to the lake. In Fig. 3, rising LOI and C:N preceding increases in dust index in the records from Bald, Marshall and Taylor Lakes are an indication of forest establishment that stabilized the landscape. Although there is nothing unusual about the configuration of Swasey Lake or its watershed, the later rise of C:N there, which nonetheless pre-dated the increase in dust index, suggests that this basin was colonized by vegetation later than the other three watersheds. In this interpretation, the early part of each lacustrine record, in which dust index values are low, is not necessarily a sign of reduced dust input. Rather, dust deposition at this time was overwhelmed by local material delivered from the unstable, recently deglaciated landscape.

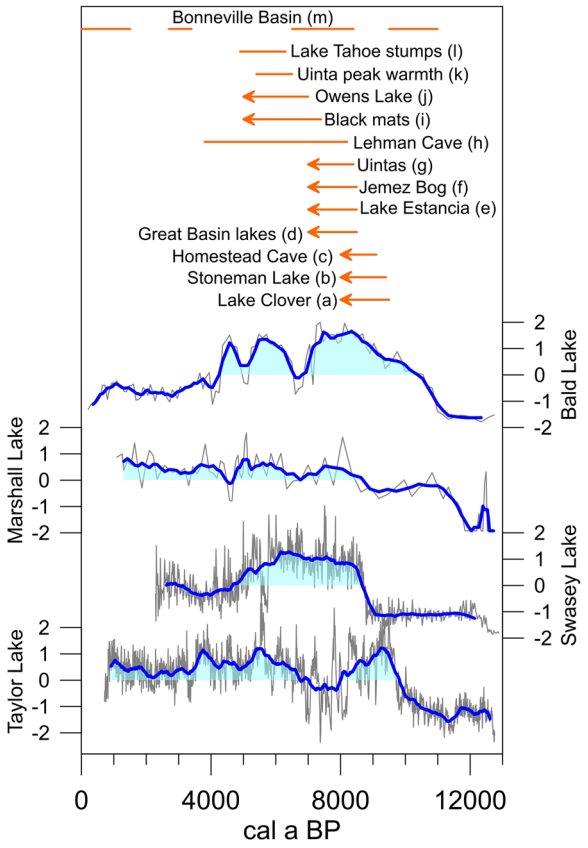

Figure 6. Time series of normalized (*z*-score) dust index in the four sediment cores compared with regional records of decreased effective moisture in the middle Holocene. Dust indices are overlain with a running mean, filled relative to 0 to emphasize long-term patterns. Orange lines represent intervals of aridity, and arrows represent increasing aridity. (a) Final desiccation of Lake Clover, Nevada (Munroe *et al.*, 2020). (b) Decreasing water level in Stoneman Lake, Arizona (Hasbargen, 1994). (c) Paleontological evidence for increasing aridity in the Bonneville Basin from Homestead Cave, Utah (Madsen *et al.*, 2001). (d) Final desiccation of Great Basin pluvial lakes (Steponaitis *et al.*, 2015). (e) Water level fall in Lake Estancia, New Mexico (Polyak and Asmerom, 2005). (f) Desiccation of Jemez Bog, New Mexico (Anderson *et al.*, 2008). (g) Pollen evidence for a transition to lodgepole pine forest in the northern Uinta Mountains (Louderback *et al.*, 2015). (h) Speleothem evidence for aridity at Lehman Cave, Nevada (Steponaitis *et al.*, 2015). (i) Aridity-related disappearance of spring-fed black mats in Arizona (Quade *et al.*, 1998). (j) Falling water in Owens Lake, California (Bacon *et al.*, 2006). (k) Peak warmth near the treeline in the northern Uinta Mountains inferred from pollen data (Munroe, 2003). (l) Sustained low water in Lake Tahoe, California and Nevada, represented by submerged tree stumps (Lindstrom, 1990). (m) Paleontological evidence from Blue Lake, Utah, for warmer conditions in the Bonneville Basin (Louderback and Rhode, 2009). [Color figure can be viewed at wileyonlinelibrary.com]

After the earliest Holocene, all four lakes were surrounded extensively by vegetation, on the basis of consistently elevated LOI and C:N signaling large inputs of terrestrial organic matter (Fig. 3). Correspondingly, values of dust index after the establishment of vegetation are more likely to faithfully record changes in dust deposition. With this in mind it is notable that after 9k cal a BP, dust index values in these records remained above average through the middle Holocene before dropping below average again ca. 5k cal a BP in Swasey and ca. 4k cal a BP in Bald Lake. In Marshall and Taylor Lakes, values oscillate near average for the remainder of the records.

An inconsistency is the low dust index values in the Taylor Lake record between 7 and 8k cal a BP (Fig. 6). However, Taylor Lake is uniquely vulnerable to the influx of local sediment because it has the largest watershed/lake area ratio (Table 1), and because a prominent fan fed by a steep drainage enters the lake along its western shore (Fig. 1). Field observations indicate that this fan is occasionally activated by major snowmelt events and summer thunderstorms, and the Taylor Lake core is punctuated by graded beds that reflect delivery of sediment by flooding events. The core was retrieved to the south of this fan (Fig. 1), meaning that when the drainage across the fan is directed towards this sector of the lake, this location is susceptible to receiving heightened influxes of local sediment. Conversely, when the drainage across the fan avulses to the north, then the southern basin of the lake is relatively protected from flooding events. As a result, to a greater extent than the other lakes, the core from Taylor Lake is more sensitive to changes in influx rather than to changes in dust delivery. In each of the coarser, clastic-rich flood layers in this core, the Ca/Ti ratio drops precipitously; several of these flood layers are clustered between 7 and 8k cal a BP when dust index values in the other lakes were higher. Furthermore, a 12-cm-thick graded bed deposited ca. 4.5k cal a BP (which was removed from the record because it was thick enough to influence the depth–age model) has notably low Ca/Ti values, providing additional support for the interpretation that the geochemistry of this core is influenced by flooding events on the fan and the location where the stream crossing the fan enters the lake. Although much smaller, a debris fan is also present on the west side of Bald Lake (Fig. 1). Transient drops to below average values of the dust index in this record ca. 4.5 and 7k cal a BP (Fig. 6) may represent a similar mechanism.

Overall, however, it is important to emphasize that (with the possible exception of Taylor Lake) the lakes in this study were not particularly sensitive to in-washing of terrestrial material after the establishment of vegetation in the surrounding watershed. Their small watersheds were not glaciated during the Holocene, none is fed by perennial streams, and all are hydrologically closed for most of the year. Moreover, the records do not exhibit prominent shifts in grain size distribution during the Holocene that would be associated with major changes in water level that repositioned the littoral zone, with its generally coarser sediment, relative to the coring site (e.g. Shuman *et al.*, 2009; Shuman and Serravezza, 2017). Therefore, interpretation of the dust index values as a first-order signal of dust deposition, rather than fluctuations in the influx of terrestrial material, is valid.

Comparison with other records

The mountains of northern Utah receive dust sourced from arid landscapes in the south-western USA, and possibly farther afield (Hahnenberger and Nicoll, 2012; Goodman *et al.*, 2019; Munroe *et al.*, 2019; Nicoll *et al.*, 2020). Therefore, the lacustrine records from the Uintas reported here are probably tracking increasing export of dust from these areas. Work has shown that dust export is controlled by the availability of fine-grained sediment for deflation (Arcusa *et al.*, 2020), which is in part related to aridity (Aarons *et al.*, 2019). A variety of paleoclimate records (Fig. 6) provide evidence of decreased effective moisture and higher temperatures in this region during the 'Altithermal Period' in the early to middle Holocene (Antevs, 1948). For instance, pollen data from sites in the Uinta Mountains indicate a transition to a lodgepole pine-dominated forest after 8.4k cal a BP (Louderback *et al.*, 2015), with peak warmth at the treeline between 6.5 and 5.4k cal a BP (Munroe, 2003). In the Great Basin to the west of the Uintas, paleontological evidence from Homestead Cave indicates drier conditions in the Bonneville Basin after 9.1k cal a BP (Madsen *et al.*, 2001), and a record from Blue Lake on the Utah/Nevada border indicates dry conditions ca. 8k cal a BP (Louderback and Rhode, 2009). Pluvial lakes in the Great Basin mostly disappeared after 8.5k cal a BP (Steponaitis *et al.*, 2015), and a detailed luminescence-based chronology indicates that Lake Clover built its final shoreline in north-eastern Nevada ca. 9.5 k a BP (Munroe *et al.*, 2020). Speleothem evidence from Lehman Cave in Nevada indicates pronounced aridity after 8.2k cal a BP, extending to the end of the record at 3.8k cal a BP (Steponaitis *et al.*, 2015). Farther west, the water level fell in Owens Lake after 7.0k cal a BP (Bacon *et al.*, 2006), and a pronounced lowstand in Lake Tahoe is evidenced by currently submerged tree stumps in growth position with calibrated radiocarbon ages from 6.3 to 4.9k cal a BP (Lindstrom, 1990). To the south of the Uintas in Arizona, pollen data signal increasing aridity at Stoneman Lake after 9.4k cal a BP (Hasbargen, 1994), and black mats related to spring-fed wetlands disappeared after 7.4k cal a BP. Similarly, in New Mexico, the water level in Lake Estancia declined after 8.5k cal a BP (Polyak and Asmerom, 2005), and Jemez Bog desiccated after 8.5k cal a BP (Anderson *et al.*, 2008). Collectively these studies testify to a regional decrease in effective moisture driven by a combination of orbital forcing, climate feedbacks and final collapse of the Laurentide Ice Sheet (Shuman and Serravezza, 2017). Increased dust index values in Uinta lakes at this time strongly suggest that the amount of dust arriving in the Uinta Mountains was elevated because of this widespread aridity.

Limitations and future directions

The dataset developed here provides a multifaceted perspective on changes in Holocene dust deposition. Nonetheless, the data have limitations that must be considered, and possibly addressed in future work. A major challenge is that a consistent set of elements was not analyzed, nor were the various sample types all analyzed with the same methodology. This reality reduces the number of elements available for formulation of dust indices. Future work building on the results presented here should use a standard methodology across all sample types.

Another issue is that the dust index is also sensitive to the influx of mineral material from the surrounding watershed. Recent studies have attempted to account for this problem by using bulk density measurements along with the slope of the depth–age model to calculate dust flux in terms of mass per year (Routson *et al.*, 2019; Arcusa *et al.*, 2020). Unfortunately, bulk density measurements were not made on these cores, so calculation of dust flux is not possible. In addition, the measurements made with the core scanner are in units of X-ray intensity, not elemental abundance, precluding the possibility

of converting the masses of sediment to masses of dust-related elements. Future work could involve direct measurement of bulk density for remaining samples from these cores using a pycnometer, or estimation of bulk density from water content (Munroe *et al.*, 2018; Munroe and Brencher, 2019). XRF scanning coupled with ICP-MS analysis could also yield calibration factors to convert X-ray intensities to elemental concentrations. Such a calibration would support mixing models with dust and local material as end-members to further quantify the dust component of lake sediments (Arcusa *et al.*, 2020). Although these steps are beyond the scope of the present study, such measures could be used in the future to allow calibration of the dust indices reported here in terms of dust flux.

Conclusions

Sediment cores from subalpine lakes in the Uinta Mountains of Utah, USA, contain a record of dust deposition during the Holocene. Given the contrasting geochemistry of dust and regolith in each watershed, the Ca/Ti and Eu/Zr ratios are used as indices for the abundance of dust in the lake sediments. Although there is some variability reflecting the unique hydrogeomorphic setting of each lake (Munroe, 2019), dust index time series are broadly consistent with one another, and signal enhanced dust deposition during the middle Holocene. This lacustrine evidence is consistent with a variety of records for increased aridity in the south-western USA at this time.

Acknowledgements. The sediment cores could not have been collected without the help of M. Devito, B. Laabs and N. Oprandy. Thanks to P. Dawson for assistance with the XRF core scanning. Support for this research was provided by National Science Foundation awards EAR-0345112 and EAR-1524476 to J. Munroe, along with a Gladstone Award from Middlebury College. The comments of Dr Mark Sweeney and an anonymous reviewer were very helpful in improving the manuscript. The authors declare no conflicts of interest.

Author contributions—Jeffrey Munroe: Conceptualization; Data Curation; Formal Analysis; Funding Acquisition; Investigation; Methodology; Project Administration; Resources; Supervision; Validation; Visualization; Writing (original draft, review, and editing). Ryan McElroy: Investigation. Sam O'Keefe: Investigation. Andrew Peters: Investigation. Luna Wasson: Investigation.

Data availability statement

The data that support the findings of this study are available from the corresponding author upon request.

Abbreviations. ICP-MS, inductively coupled mass emission spectrometry; ICP-OES, inductively coupled plasma optical emission spectrometry; LOI, loss on ignition; XRF, X-ray fluorescence.

References

Aarons SM, Arvin LJ, Aciego SM *et al.* 2019. Competing droughts affect dust delivery to Sierra Nevada. *Aeolian Research* **41**.

Aciego SM, Riebe CS, Hart SC *et al.* 2017. Dust outpaces bedrock in nutrient supply to montane forest ecosystems. *Nature Communications* **8** 14800.

Anderson RS, Jass RB, Toney JL *et al.* 2008. Development of the mixed conifer forest in northern New Mexico and its relationship to Holocene environmental change. *Quaternary Research* **69**: 263–275.

Antevs EV. 1948. The Great Basin, with emphasis on glacial and postglacial times; Climatic changes and pre-white man. *Bulletin of the University of Utah* **38**: 168–191.

Arcusa SH, McKay NP, Routson CC *et al.* 2020. Dust-drought interactions over the last 15,000 years: A network of lake sediment records from the San Juan Mountains, Colorado. *The Holocene* **30**: 559–574.

Arvin LJ, Riebe CS, Aciego SM *et al.* 2017. Global patterns of dust and bedrock nutrient supply to montane ecosystems. *Science Advances 3: eaao1* 588.

Atwood WW. 1908. Lakes of the Uinta Mountains. *Bulletin of the American Geographical Society* **40**: 12–17.

Atwood WW. 1909. *Glaciation of the Uinta and Wasatch mountains*. US Government Printing Office: Washington.

Bacon SN, Burke RM, Pezzopane SK *et al.* 2006. Last Glacial Maximum and Holocene lake levels of Owens Lake, eastern California, USA. *Quaternary Science Reviews* **25**: 1264–1282.

Ballantyne AP, Brahney J, Fernandez D *et al.* 2011. Biogeochemical response of alpine lakes to a recent increase in dust deposition in the Southwestern, US. *Biogeosciences* **8**: 2689–2706.

Blaauw M. 2010. Methods and code for 'classical' age-modelling of radiocarbon sequences. *Quaternary Geochronology* **5**: 512–518.

Bockheim JG, Koerner D. 1997. Pedogenesis in Alpine Ecosystems of the Eastern Uinta Mountains, Utah, U.S.A. *Arctic and Alpine Research* **29**: 164–172.

Bockheim JG, Munroe JS. 2014. Organic carbon pools and genesis of alpine soils with permafrost: a review. *Arctic, Antarctic, and Alpine Research* **46**: 987–1006.

Bockheim JG, Munroe JS, Douglass D *et al.* 2000. Soil development along an elevational gradient in the southeastern Uinta Mountains, Utah, USA. *CATENA* **39**: 169–185.

Bradley WH. 1936. *Geomorphology of the North Flank of the Uinta Mountains*. US Government Printing Office: Washington.

Brahney J, Ballantyne AP, Kociolek P *et al.* 2014. Dust mediated transfer of phosphorus to alpine lake ecosystems of the Wind River Range, Wyoming, USA. *Biogeochemistry* **120**: 259–278.

Brahney J, Ballantyne AP, Sievers C *et al.* 2013. Increasing Ca^{2+} deposition in the western US: the role of mineral aerosols. *Aeolian Research* **10**: 77–87.

Dahms DE. 1993. Mineralogical evidence for eolian contribution to soils of late Quaternary moraines, Wind River Mountains, Wyoming, USA. *Geoderma* **59**: 175–196.

Dean WE Jr. 1974. Determination of carbonate and organic matter in calcareous sediments and sedimentary rocks by loss on ignition; comparison with other methods. *Journal of Sedimentary Petrology* **44**: 242–248.

Dehler CM, Porter SM, De Grey LD *et al.* 2007 *The Neoproterozoic Uinta Mountain Group Revisited; a Synthesis of Recent Work on the Red Pine Shale and Related Undivided Clastic Strata, Northeastern Utah, USA*. Special Publication. Society for Sedimentary Geology 86; 151–166.

Duniway MC, Pfennigwerth AA, Fick SE *et al.* 2019. Wind erosion and dust from US drylands: a review of causes, consequences, and solutions in a changing world. *Ecosphere* **10** e02650.

Flagg CB, Neff JC, Reynolds RL *et al.* 2014. Spatial and temporal patterns of dust emissions (2004–2012) in semi-arid landscapes, southeastern Utah, USA. *Aeolian Research* **15**: 31–43.

Kandakji T, Gill TE, Lee JA. 2020. Identifying and characterizing dust point sources in the southwestern United States using remote sensing and GIS. *Geomorphology* **353** 107019.

Goodman MM, Carling GT, Fernandez DP *et al.* 2019. Trace element chemistry of atmospheric deposition along the Wasatch Front (Utah, USA) reflects regional playa dust and local urban aerosols. *Chemical Geology* **530**.

Hahnenberger M, Nicoll K. 2012. Meteorological characteristics of dust storm events in the eastern Great Basin of Utah, U.S.A. *Atmospheric Environment* **60**: 601–612.

Hasbargen J. 1994. A Holocene paleoclimatic and environmental record from Stoneman Lake, Arizona. *Quaternary Research* **42**: 188–196.

Heindel RC, Putman AL, Murphy SF *et al.* 2020. Atmospheric dust deposition varies by season and elevation in the Colorado Front

Range, USA. *Journal of Geophysical Research – Earth Surface* **125** e2019JF005436.
Laabs BJC, Refsnider KA, Munroe JS *et al*. 2009. Latest Pleistocene glacial chronology of the Uinta Mountains: support for moisture-driven asynchrony of the last deglaciation. *Quaternary Science Reviews* **28**: 1171–1187.
Lawrence CR, Neff JC. 2009. The contemporary physical and chemical flux of aeolian dust: A synthesis of direct measurements of dust deposition. *Chemical Geology* **267**: 46–63.
Lawrence CR, Neff JC, Farmer GL *et al*. 2011. The accretion of aeolian dust in soils of the San Juan Mountains, Colorado, USA. *Journal of Geophysical Research: Earth Surface* **116**: F02013.
Lawrence CR, Reynolds RL, Ketterer ME *et al*. 2013. Aeolian controls of soil geochemistry and weathering fluxes in high-elevation ecosystems of the Rocky Mountains, Colorado. *Geochimica et Cosmochimica Acta* **107**: 27–46.
Lindstrom S. 1990. Submerged tree stumps as indicators of mid-Holocene aridity in the Lake Tahoe region. *Journal of California and Great Basin Anthropology* **12**: 146–157.
Litaor MI. 1987. The influence of eolian dust on the genesis of alpine soils in the Front Range, Colorado. *Soil Science Society of America Journal* **51**: 142–147.
Louderback LA, Rhode D, Madsen DB *et al*. 2015. Rapid vegetation shifts in the Uinta Mountains (Utah and Wyoming, USA) during the Late Pleistocene and Holocene. *Palaeogeography, Palaeoclimatology, Palaeoecology* **438**: 327–343.
Louderback LA, Rhode DE. 2009. 15,000 Years of vegetation change in the Bonneville basin: the Blue Lake pollen record. *Quaternary Science Reviews* **28**: 308–326.
Madsen DB, Rhode D, Grayson DK *et al*. 2001. Late Quaternary environmental change in the Bonneville Basin, Western USA. *Palaeogeography, Palaeoclimatology, Palaeoecology* **167**: 243–271.
McLennan SM. 1989. Rare earth elements in sedimentary rocks: influence of provenance and sedimentary processes. *Reviews in Mineralogy* **21**: 169–200.
Muhs DR, Benedict JB. 2006. Eolian additions to late Quaternary alpine soils, Indian Peaks Wilderness Area, Colorado Front Range. *Arctic, Antarctic, and Alpine Research* **38**: 120–130.
Munroe J, Brencher Q. 2019. Holocene carbon burial in lakes of the Uinta Mountains, Utah, USA. *Quaternary* **2**: 13.
Munroe JS. 2003. Holocene timberline and palaeoclimate of the northern Uinta Mountains, northeastern Utah, USA. *The Holocene* **13**: 175–185.
Munroe JS. 2006. Investigating the spatial distribution of summit flats in the Uinta Mountains of northeastern Utah, USA. *Geomorphology* **75**: 437–449.
Munroe JS. 2007. Properties of alpine soils associated with well-developed sorted polygons in the Uinta Mountains, Utah, U.S.A. *Arctic, Antarctic, and Alpine Research* **39**: 578–591.
Munroe JS. 2012. Physical, chemical, and thermal properties of soils across a forest-meadow ecotone in the Uinta Mountains, Northeastern Utah, U.S.A. *Arctic, Antarctic, and Alpine Research* **44**: 95–106.
Munroe JS. 2014. Properties of modern dust accumulating in the Uinta Mountains, Utah, USA, and implications for the regional dust system of the Rocky Mountains. *Earth Surface Processes and Landforms* **39**: 1979–1988.
Munroe JS. 2019. Hydrogeomorphic controls on Holocene lacustrine loss-on-ignition records. *Journal of Paleolimnology* **61**: 53–68.
Munroe JS, Attwood EC, O'Keefe SS *et al*. 2015. Eolian deposition in the alpine zone of the Uinta Mountains, Utah, USA. *CATENA* **124**: 119–129.
Munroe JS, Bigl MF, Silverman AE *et al*. 2018. Records of late Quaternary environmental change from high-elevation lakes in the Ruby Mountains and East Humboldt Range, Nevada. In *From Saline to Freshwater: the Diversity of Western Lakes in Space and Time*, Starratt SW, Rosen MR (eds). Geological Society of America Special Paper 536.
Munroe JS, Laabs BJC 2009. *Glacial Geologic Map of the Uinta Mountains Area, Utah and Wyoming*. Utah Geological Survey Miscellaneous Publication 09-4DM, Scale 1: 100,000.
Munroe JS, Laabs BJC. 2017. Combining radiocarbon and cosmogenic ages to constrain the timing of the last glacial-interglacial transition in the Uinta Mountains, Utah, USA. *Geology* **45**: 171–174.
Munroe JS, Laabs BJC. 2020. Multiproxy lacustrine records of post-glacial environmental change from the Uinta Mountains, Utah, USA. *GSA Bulletin* **132**: 48–64.
Munroe JS, Laabs BJC, Shakun JD *et al*. 2006. Latest Pleistocene advance of alpine glaciers in the southwestern Uinta Mountains, Utah, USA: evidence for the influence of local moisture sources. *Geology* **34**: 841–844.
Munroe JS, Mickelson DM. 2002. Last Glacial Maximum equilibrium-line altitudes and paleoclimate, northern Uinta Mountains, Utah, U.S.A. *Journal of Glaciology* **48**: 257–266.
Munroe JS, Norris ED, Carling GT *et al*. 2019. Isotope fingerprinting reveals western North American sources of modern dust in the Uinta Mountains, Utah, USA. *Aeolian Research* **38**: 39–47.
Munroe JS, Walcott CK, Amidon WH *et al*. 2020. A top-to-bottom luminescence-based chronology for the post-LGM regression of a Great Basin pluvial lake. *Quaternary* **3**: 11.
Neff JC, Ballantyne AP, Farmer GL *et al*. 2008. Increasing eolian dust deposition in the western United States linked to human activity. *Nature Geoscience* **1**: 189–195.
Nesbitt HW, Markovics G. 1997. Weathering of granodioritic crust, long-term storage of elements in weathering profiles, and petrogenesis of siliciclastic sediments. *Geochimica et Cosmochimica Acta* **61**: 1653–1670.
Nicoll K, Hahnenberger M, Goldstein HL. 2020. Dust in the wind' from source-to-sink: analysis of the 14–15 April 2015 storm in Utah. *Aeolian Research* **46**.
Painter TH, Barrett AP, Landry CC *et al*. 2007. Impact of disturbed desert soils on duration of mountain snow cover. *Geophysical Research Letters* **34**. L12502–L12502.
Painter TH, Deems JS, Belnap J *et al*. 2010. Response of Colorado River runoff to dust radiative forcing in snow. *Proceedings of the National Academy of Sciences of the United States of America* **107**: 17125–17130.
Polyak VJ, Asmerom Y. 2005. Orbital control of long-term moisture in the southwestern USA. *Geophysical Research Letters* 32.
Quade J, Forester RM, Pratt WL *et al*. 1998. Black mats, spring-fed streams, and late-glacial-age recharge in the southern Great Basin. *Quaternary Research* **49**: 129–148.
Rea P, Ma L, Gill TE *et al*. 2020. Tracing gypsiferous White Sands aerosols in the shallow critical zone in the northern Sacramento Mountains, New Mexico using Sr/Ca and $^{87}Sr/^{86}Sr$ ratios. *Geoderma* **372**.
Reasoner MA. 1993. Equipment and procedure improvements for a lightweight, inexpensive, percussion core sampling system. *Journal of Paleolimnology* **8**: 273–281.
Reynolds RL, Mordecai JS, Rosenbaum JG *et al*. 2010. Compositional changes in sediments of subalpine lakes, Uinta Mountains (Utah): evidence for the effects of human activity on atmospheric dust inputs. *Journal of Paleolimnology* **44**: 161–175.
Reynolds RL, Munson SM, Fernandez D *et al*. 2016. Concentrations of mineral aerosol from desert to plains across the central Rocky Mountains, western United States. *Aeolian Research* **23**: 21–35.
Roe G. 2009. On the interpretation of Chinese loess as a paleoclimate indicator. *Quaternary Research* **71**: 150–161.
Routson CC, Arcusa SH, McKay NP *et al*. 2019. A 4,500-year-long record of southern Rocky Mountain dust deposition. *Geophysical Research Letters* **46**: 8281–8288.
Routson CC, Overpeck JT, Woodhouse CA *et al*. 2016. Three millennia of southwestern North American dustiness and future implications. *PLoS ONE* **11** e0149573.
Sears J, Graff P, Holden G. 1982. Tectonic evolution of lower Proterozoic rocks, Uinta Mountains, Utah and Colorado. *Geological Society of America Bulletin* **93**: 990–997.
Shaw JD, Long JN. 2007. Forest Ecology and Biogeography of the Uinta Mountains, U.S.A. *Arctic, Antarctic, and Alpine Research* **39**: 614–628.
Shuman B, Henderson AK, Colman SM *et al*. 2009. Holocene lake-level trends in the Rocky Mountains, U.S.A. *Quaternary Science Reviews* **28**: 1861–1879.
Shuman BN, Serravezza M. 2017. Patterns of hydroclimatic change in the Rocky Mountains and surrounding regions since the last glacial maximum. *Quaternary Science Reviews* **173**: 58–77.
Skiles SM, Mallia DV, Hallar AG *et al*. 2018. Implications of a shrinking Great Salt Lake for dust on snow deposition in the Wasatch Mountains,

UT, as informed by a source to sink case study from the 13–14 April 2017 dust event. *Environmental Research Letters* 13.

Skiles SM, Painter T. 2017. Daily evolution in dust and black carbon content, snow grain size, and snow albedo during snowmelt, Rocky Mountains, Colorado. *Journal of Glaciology* **63**: 118–132.

Skiles SM, Painter TH, Belnap J *et al*. 2015. Regional variability in dust-on-snow processes and impacts in the Upper Colorado River Basin. *Hydrological Processes* **29**: 5397–5413.

Skiles SM, Painter TH, Deems JS *et al*. 2012. Dust radiative forcing in snow of the Upper Colorado River Basin: 2. Interannual variability in radiative forcing and snowmelt rates. *Water Resources Research* **48**.

Steponaitis E, Andrews A, McGee D *et al*. 2015. Mid-Holocene drying of the U.S. Great Basin recorded in Nevada speleothems. *Quaternary Science Reviews* **127**: 174–185.

Urban FE, Reynolds RL, Fulton R. 2009. The dynamic interaction of climate, vegetation, and dust emission, Mojave Desert, USA, *Arid Environments and Wind Erosion*. Nova Science Publishers: New York; 243–267.